Volumetric imaging of turbulent reactive flows at kHz based on computed tomography

Xuesong Li and Lin Ma*

Department of Aerospace and Ocean Engineering, Virginia Tech, Blacksburg, Virginia 24060, USA
*LinMa@vt.edu

Abstract: Diagnostics with three-dimensional (3D) spatial resolution and rapid temporal resolution have been long desired to resolve the complicated turbulence-chemistry interactions. This paper describes a method based on based on tomographic chemiluminescence (TC) to address this diagnostic need. The TC technique used multiple cameras to simultaneously record CH* chemiluminescence emitted by turbulent flames from different view angles. A 3D tomographic algorithm was then applied to reconstruct the instantaneous flame structures volumetrically. Both experimental and computational studies have been conducted to demonstrate and validate the 3D measurements. Experimental results were obtained instantaneously at kHz temporal rate, in a volume of 16 × 16 × 16 cm^3, and with a spatial resolution estimated to be 2~3 mm. Computations were conducted to simulate the experimental conditions for comparison and validation.

©2014 Optical Society of America

OCIS codes: (100.6890) Three-dimensional image processing; (100.6950) Tomographic image processing; (120.1740) Combustion diagnostics; (300 2140) Emission.

References and links

1. R. S. Barlow, "Laser diagnostics and their interplay with computations to understand turbulent combustion," Proc. Combust. Inst. **31**(1), 49–75 (2007).
2. L. Ma, "High Speed Imaging in Reactive Flows Using Hyperspectral Tomography and Photodissociation Spectroscopy," in *Laser Applications to Chemical, Security and Environmental Analysis*, (Optical Society of America, OSA Technical Digest Series, Paper LWA3, 2010)
3. L. Ma, X. Li, S. Roy, A. Caswell, J. R. Gord, D. Plemmons, X. An, and S. T. Sanders, "Demonstration of High Speed Imaging in Practical Propulsion Systems Using Hyperspectral Tomography," in *Laser Applications to Chemical, Security and Environmental Analysis*, (Optical Society of America, OSA Technical Digest, paper LM1B.5., 2012)
4. R. Wellander, M. Richter, and M. Aldén, "Time resolved, 3D imaging (4D) of two phase flow at a repetition rate of 1 kHz," Opt. Express **19**(22), 21508–21514 (2011).
5. J. Hult, A. Omrane, J. Nygren, C. F. Kaminski, B. Axelsson, R. Collin, P. E. Bengtsson, and M. Alden, "Quantitative three-dimensional imaging of soot volume fraction in turbulent non-premixed flames," Exp. Fluids **33**(2), 265–269 (2002).
6. L. Ma, X. Li, S. T. Sanders, A. W. Caswell, S. Roy, D. H. Plemmons, and J. R. Gord, "50-kHz-rate 2D imaging of temperature and H_2O concentration at the exhaust plane of a J85 engine using hyperspectral tomography," Opt. Express **21**(1), 1152–1162 (2013).
7. F. Li, X. Yu, H. Gu, Z. Li, Y. Zhao, L. Ma, L. Chen, and X. Chang, "Simultaneous Measurements of Multiple Flow Parameters for Scramjet Characterization Using Tunable Diode-laser Sensors," Appl. Opt. **50**(36), 6697–6707 (2011).
8. D. P. Correia, P. Ferrao, and A. Caldeira-Pires, "Advanced 3D emission tomography flame temperature sensor," Combust. Sci. Technol. **163**(1), 1–24 (2001).
9. J. Floyd, P. Geipel, and A. M. Kempf, "Computed Tomography of Chemiluminescence (CTC): Instantaneous 3D measurements and Phantom studies of a turbulent opposed jet flame," Combust. Flame **158**(2), 376–391 (2011).
10. R. Snyder and L. Hesselink, "Measurement of mixing fluid flows with optical tomography," Opt. Lett. **13**(2), 87–89 (1988).
11. W. Cai, X. Li, F. Li, and L. Ma, "Numerical and experimental validation of a three-dimensional combustion diagnostic based on tomographic chemiluminescence," Opt. Express **21**(6), 7050–7064 (2013).
12. Y. Hardalupas and M. Orain, "Local measurements of the time-dependent heat release rate and equivalence ratio using chemiluminescent emission from a flame," Combust. Flame **139**(3), 188–207 (2004).
13. Y. Hardalupas, M. Orain, C. S. Panoutsos, A. Taylor, J. Olofsson, H. Seyfried, M. Richter, J. Hult, M. Alden, F. Hermann, and J. Klingmann, "Chemiluminescence sensor for local equivalence ratio of reacting mixtures of fuel and air (FLAMESEEK)," Appl. Therm. Eng. **24**, 1619–1632 (2004).

#202046 - $15.00 USD Received 5 Dec 2013; revised 27 Jan 2014; accepted 27 Jan 2014; published 21 Feb 2014
(C) 2014 OSA

14. O. Stein, A. M. Kempf, and J. Janicka, "LES of the sydney swirl flame series: An initial investigation of the fluid dynamics," Combust. Sci. Technol. **179**, 173–189 (2007).
15. J. Floyd and A. M. Kempf, "Computed Tomography of Chemiluminescence (CTC): High resolution and instantaneous 3-D measurements of a Matrix burner," Proc. Combust. Inst. **33**(1), 751–758 (2011).
16. N. Denisova, P. Tretyakov, and A. Tupikin, "Emission tomography in flame diagnostics," Combust. Flame **160**(3), 577–588 (2013).
17. N. A. Worth and J. R. Dawson, "Tomographic reconstruction of OH* chemiluminescence in two interacting turbulent flames," Meas. Sci. Technol. **24**(2), 024013 (2013).
18. W. Cai, A. J. Wickersham, and L. Ma, "Three-Dimensional Combustion Diagnostics Based on Computed Tomography of Chemiluminescence," in *51st AIAA Aerospace Sciences Meeting Including the New Horizons Forum and Aerospace Exposition,* (Dallas Region, TX, 2013).
19. X. Li and L. Ma, Three-Dimensional Measurements of Turbulent Jet Flames at kHz Rate Based on Tomographic Chemiluminescence " in *AIAA SciTech 2014, Paper AIAA-2014–0735,* (National Harbor, MD, 2014).
20. W. Cai and L. Ma, "Comparison of approaches based on optimization and algebraic iteration for binary tomography," Comput. Phys. Commun. **181**(12), 1974–1981 (2010).
21. W. Cai, D. J. Ewing, and L. Ma, "Investigation of temperature parallel simulated annealing for optimizing continuous functions with application to hyperspectral tomography," Appl. Math. Comput. **217**(12), 5754–5767 (2011).
22. L. Ma, L. Kranendonk, W. Cai, Y. Zhao, and J. Baba, "Application of simulated annealing for simultaneous retrieval of particle size distribution and refractive index," J. Aerosol Sci. **2009**, 588–596 (2009).
23. X. An, T. Kraetschmer, K. Takami, S. T. Sanders, L. Ma, W. Cai, X. Li, S. Roy, and J. R. Gord, "Validation of temperature imaging by H_2O absorption spectroscopy using hyperspectral tomography in controlled experiments," Appl. Opt. **50**(4), A29–A37 (2011).
24. L. Ma, X. Li, S. T. Sanders, A. W. Caswell, S. Roy, D. H. Plemmons, and J. R. Gord, "50-kHz-rate 2D imaging of temperature and H_2O concentration at the exhaust plane of a J85 engine using hyperspectral tomography," Opt. Express **21**(1), 1152–1162 (2013).
25. G. Frieder and G. T. Herman, "Resolution in reconstructing objects from electron micrographs," J. Theor. Biol. **33**(1), 189–211 (1971).
26. G. T. Herman and S. Rowland, "Resolution in algebraic reconstruction techchqique an experimental investigation of the resolving power of an algebraic picture reconstruction techniuqe," J. Theor. Biol. **33**, 213–223 (1971).
27. V. Weber, J. Bruebach, R. L. Gordon, and A. Dreizler, "Pixel-based characterisation of CMOS high-speed camera systems," Appl. Phys. B **103**(2), 421–433 (2011).
28. W. Cai, X. Li, Y. Cao, J. Wang, and L. Ma, "Practical aspects of three-dimensional flame imaging using tomographic chemiluminescence " in *AIAA SciTech 2014, Paper AIAA-2014–0394,* (National Harbor, MD, USA, 2014).
29. M. Kang, X. Li, and L. Ma, "Calibration of Fiber Bundles for Flow and Combustion Measurements," in *AIAA SciTech 2014, Paper AIAA-2014–0397,* (National Harbor, MD, 2014).
30. J. Kitzhofer, T. Nonn, and C. Bruecker, "Generation and visualization of volumetric PIV data fields," Exp. Fluids **51**(6), 1471–1492 (2011).

1. Introduction

Three-dimensional (3D) spatial structures and rapid temporal dynamics are inherent to turbulent flames. Combustion diagnostics that can resolve such 3D spatial structures with adequate temporal resolution have therefore been long desired [1]. However, it is a tremendous challenge to develop such diagnostic techniques both due to fundamental reasons (e.g., the multi-spatial and -temporal scales of interest) and also practical reasons (e.g., harsh environments and hardware limit). Possible strategies seem to be very limited and existing efforts can be broadly divided into two categories [2, 3]. The first category of techniques obtains 3D measurements by rapidly scanning a 2D technique, any 2D technique (at least conceptually) such as planar Mie scattering [4], planar laser induced incandescence [5], or even 2D absorption-based tomography [6, 7]. The second category of techniques obtains 3D measurements volumetrically by performing a 3D tomography [8–11]. These two strategies have both fundamental differences (in terms of spatial resolution, temporal resolution, field of view, etc.) and practical differences (in terms of equipment cost, alignment difficulty, optical access, etc.). A comprehensive comparison of these aspects is out of the scope of current paper (though highly valuable).

This paper focuses on the tomographic strategy, particularly instantaneous flame measurements based on tomographic chemiluminescence (TC). Compared with other laser-based combustion diagnostics, the TC technique enjoys several important advantages. The TC technique is relatively simple. It relies on signals naturally emitted by the flame and circumvents the need of costly and delicate laser equipment typically required by other

#202046 - $15.00 USD Received 5 Dec 2013; revised 27 Jan 2014; accepted 27 Jan 2014; published 21 Feb 2014
(C) 2014 OSA

diagnostics. Yet the TC technique offers the prospect of measuring many critical flame quantities that are very challenging for other diagnostics, including the rate of heat release [12], local equivalence ratio [13], and flame topography [14]. These quantities are of great value for the development and validation of advanced models [9, 15]. Such prospective capabilities have motivated several investigations on the use of TC for volumetric combustion measurements. Denisova et al discussed a new tomographic algorithms and reported validation results on axially symmetric flames [16]. Worth et al demonstrated TC as a powerful tool for resolving large scale vortex-flame dynamics by measuring mean and phased-averaged OH* distributions [17]. Cai et al investigated the performance of various tomographic algorithms and the spatial resolution of TC using stable and patterned flames [11, 18, 19]. Floyd et al performed phantoms studies of TC and demonstrated 3D flame measurements at tens of frames per second rate [9, 15]. Based on these past efforts, this work describes the demonstration and validation of volumetric flame measurements based on TC at kHz temporal rate (i.e., with sub-ms exposure time and kHz frame rate), with an special focus on the quantification of the spatial resolution and validation of the measurements.

2. TC technique fundamentals

Figure 1 illustrates the mathematical formulation of the TC technique. Denote the 3D distribution of the chemiluminescence species (CH* in this work) as *F(x,y,z)*, which is discretized into voxels in the measurement volume. Line-of-sight images of *F* are measured as 2D *projections* on cameras, and the projections formed depend on the location and orientation of the cameras, specified by r (distance), θ (azimuth angle), and ϕ (inclination angle). The relationship between a projection (P) and F is:

$$P(r,\theta,\phi) = \sum_{x_i,y_i,z_i} F(x_i,y_i,z_i)\cdot PSF(x_i,y_i,z_i;r,\theta,\phi) \qquad (1)$$

where x_i, y_i, z_i represent the voxel centered at (x_i, y_i, z_i); and *PSF* is the *point spread function* defined as the projection formed by a point-source located at (x_i, y_i, z_i) with unity intensity.

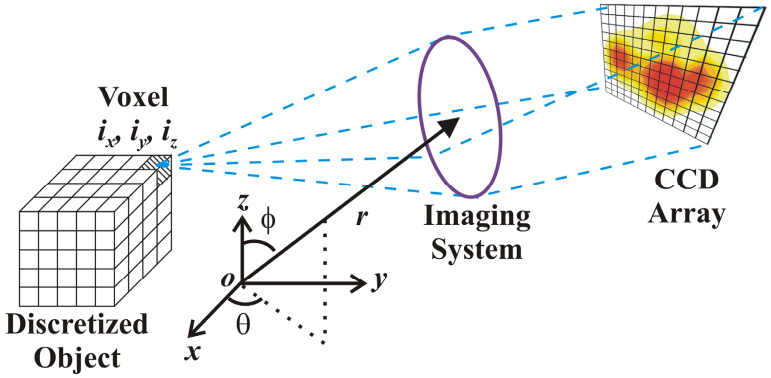

Fig. 1. Concept and mathematical formulation of TC.

Physically, Eq. (1) states that the projection is a weighted summation of the *PSF* across all voxels, and the weights are the value of the sought distribution. In this work the PSF was obtained using a Monte Carlo method. Calculating the *PSF* is computationally intensive for the scale of problem under consideration in this work, and a Monte Carlo method was adopted to calculate the *PSFs* due to its flexibility and relative ease of programming. Photons were generated at each voxel in random directions one by one. The program then tracked the propagation of each photon through all the optical elements in the imaging system until it landed on a pixel on the camera chip. The location of the pixel was then recorded. By generating a large number of photons, a distribution of their landing pixels was obtained and was used as the *PSF* for the given pixel after normalization by the number of photons

#202046 - $15.00 USD Received 5 Dec 2013; revised 27 Jan 2014; accepted 27 Jan 2014; published 21 Feb 2014
(C) 2014 OSA

generated on this given pixel. After obtaining the *PSF*, the 3D TC problem is then formulated as: given a set of projections (*P*s) measured at various distances and orientations, find *F(x,y,z)*.

Various algorithms have been proposed to solve this problem [11, 16, 20, 21] and this work adopted an algorithm based on simulated annealing as described in [11] (code named TISA, Tomographic Inversion by Simulated Annealing). The algorithm has been demonstrated effective to solve other types of inversion problems in combustion measurements [22–24]. A brief summary of the algorithm is summarized here to facilitate discussion and detailed description can be found elsewhere [22–24]. The TISA algorithm formulates the tomographic reconstruction into the following minimization problem:

$$\min \sum_{r,\theta,\Phi} [P_m(r,\theta,\phi) - P_c(r,\theta,\phi)]^2 \text{ with respect to } F(x,y,z) \qquad (2)$$

where P_m represents the measured projections at (r, θ, ϕ), P_c the projection calculated at (r, θ, ϕ) with a given distribution according to Eq. (1), and the summation runs over all locations and orientations of measurements. Equation (2) essentially seeks the F that best (in the least squares sense) reproduces the projection measurements. Solving Eq. (2) is nontrivial due to the scale of the problem, and the Simulated Annealing [11] algorithm, a stochastic minimization method, has been shown to solve Eq. (2) effectively both in this work our previous work involving complicated flow and combustion tomographic reconstructions.

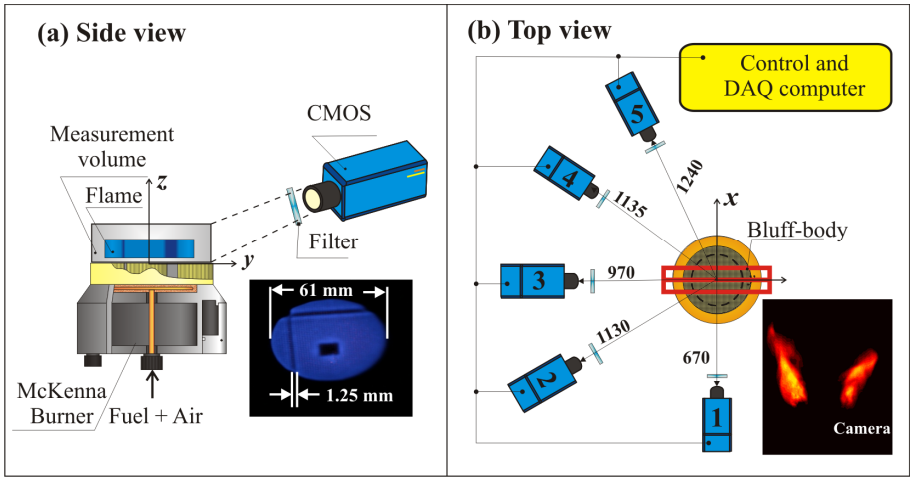

Fig. 2. Experimental setup. Panel (a). side view with a stable flame. Panel (b). top view with a turbulent flame.

Validation of the TISA algorithm was conducted using an experimental setup as shown in Fig. 2(a). A McKenna burner was customized to generate stable flame patterns with controlled spatial features, so that projections can be measured sequentially with one camera. An example flame pattern was shown in the lower right corner of Panel (a) with an overall size of 61 mm and a minimum spatial feature controlled to 1.25 mm, created by the McKenna burner and a honeycomb. The McKenna burner generated a stable and disk-like flame with a diameter of ~61 mm and a thickness of ~1 mm. A honeycomb was then placed on the McKenna burner to create the controlled flame features shown here. The honeycomb's cells are squares with size of 1.25 × 1.25 mm and certain cells were blocked to create the desired asymmetric pattern as shown, for the demonstration and validation of the 3D tomographic technique.. Projections of the flame were recorded using one PCO sensicam camera equipped with a Nikon Macro lens (105 mm f/2.8) from various view angles sequentially, based on which the TISA algorithm was applied to reconstruct the target flame in 3D. The controlled flame pattern eventually became blurred due to diffusion and convection as the flame propagates upwards. Therefore the controlled pattern was only valid within a certain range of

#202046 - $15.00 USD Received 5 Dec 2013; revised 27 Jan 2014; accepted 27 Jan 2014; published 21 Feb 2014
(C) 2014 OSA

HAB (height above burner). We studied this dependence by analyzing static photographs of the flame, and found that the controlled pattern was valid for HAB less than about 1.25 mm. The results shown in Fig. 3 used the portion of the flame that within an HAB of 1 mm.

Such patterned flames enable the experimental validation of the TISA algorithm both qualitatively (e.g., the overall flame structure) and quantitatively (e.g., the size, shape, and location of the spatial patterns). For the McKenna flame measurements, the measurement volume was taken as a cylindrical region with a diameter of 67.5 mm and a height of 1 mm to encompass the flame. The measurement volume was descretized into 54 (x direction) × 54 (y direction) × 4 (z direction) voxels, resulting in a total of 11,664 voxels. Each voxel has a dimension of 1.25 mm in both the x and y directions and 0.25 mm in the z direction. The size of the voxels is limited by both practical and fundamental factors. Practically, the computational cost and memory requirement scales to the third power of voxel size (or more precisely, the inversion of voxel size). Fundamentally, the number of unknowns in the tomography problem also scales to the third power of the inverse of the voxel size. So if the voxel size becomes too small, it leads to more unknowns than the available equations (i.e., number of pixels in the projections), the tomography problem becomes under-determined.

Such flames with controlled patterns also allowed the quantitative study of TC's spatial resolution. Here we used the finest spatial feature (1.25 mm) created in the flame as shown in Fig. 2(a), to quantify the spatial resolution. Figure 3 shows the width of this finest feature reconstructed by the TC technique with various numbers of projections. The reconstructed width was determined by calculating the gradient of the 3D reconstruction and locating the sharpest CH* concentration change. The reconstructed width may vary along the length of this feature. Therefore, multiple values were obtained and Fig. 3 shows the median (the solid symbols) and standard deviation (the error bars).

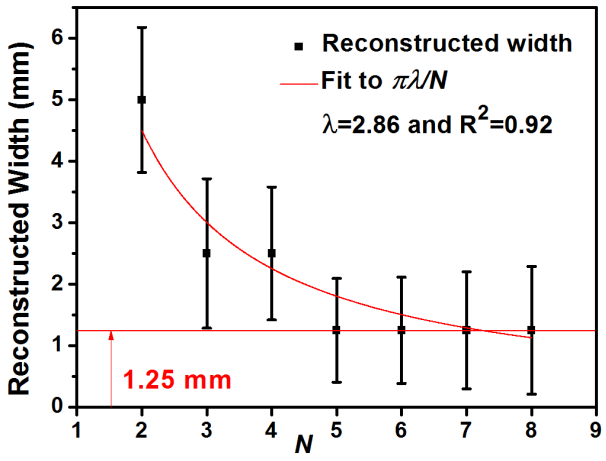

Fig. 3. Spatial resolution with various numbers of views.

Figure 3 shows the spatial resolution of the TC technique improves as projections at increasing number of views (N) are used in the reconstruction. For this particular flame as shown in Fig. 2(a), the TC technique can resolve its finest 1.25 mm feature with 8 views. The same trend as shown in Fig. 3 has been observed by numerical simulations. Besides experimental and numerical results, theoretical results are also available to predict the spatial resolution of tomographic reconstructions. For example, the Fourier Slice Theorem [25, 26] predicts the spatial resolution to scale as $\pi\lambda/N$, where λ is a characteristic spatial scale. A fit of the experimental data in Fig. 3 according to this theorem indicates that the data were reasonably captured. Note that the spatial resolution usually is defined by the minimum distance between line pairs. Here the thickness of a feature was used instead due to the experimental difficulty of creating controlled line pairs in gaseous and/or combustion flows.

#202046 - $15.00 USD Received 5 Dec 2013; revised 27 Jan 2014; accepted 27 Jan 2014; published 21 Feb 2014
(C) 2014 OSA

A method to overcome such difficulty will definitely benefit not only this work, but also a wide range of other flow/flame diagnostics.

These results demonstrate experimentally, numerically, and theoretically that TC is capable of enabling 3D flame measurements 1) with sub-mm spatial resolution, and 2) with a limited number of views that is practically feasible for combustion systems. As shown in Fig. 3, better spatial resolution can be achieved with further increase of the number of views, and we are fabricating new burners that can generate flames with finer controlled spatial features to provide experimental validation.

3. Turbulent flame measurement

After the validation study discussed above, we demonstrated TC in turbulent flames at kHz rate. The experimental setup is shown in Fig. 2(b). The setup is similar to the validation experiment. The major difference was the replacement of the McKenna flame with jet flames stabilized by bluff bodies. Five CMOS cameras (Photron SA4 and SA6), as shown, were applied to measure projections from five views simultaneously (*r* for each camera is shown in units of mm). Measurements were made with various flames and view arrangements up to 5 kHz (5 kHz frame rate and 0.2 ms exposure time). The temporal rate was largely determined by the intensity of the flame and *r*, so projections can be measured with sufficient SNR). Use of intensifiers and a different set of lenses can further enhance the temporal rate. Before each measurement, the cameras were calibrated using a uniform illuminator on a pixel-by-pixel basis as described in [27], and the location and orientation of cameras were determined by a calibration plate and a view registration algorithm [28, 29].

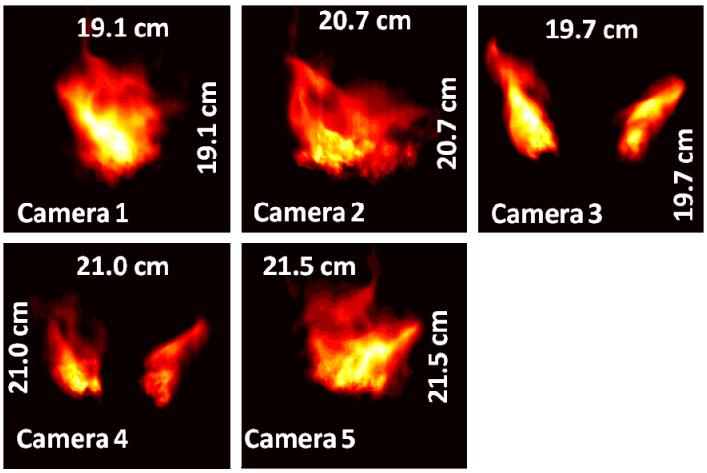

Fig. 4. Five simultaneously projections.

Figure 4 shows an example set of projections simultaneously measured by the five cameras at 1 kHz in a jet flame stabilized by a V-gutter bluff-body. The jet diameter was 3 mm, and the Reynolds number defined by the jet diameter was 10,770. The volume imaged by all five cameras was about 20 × 20 × 20 cm^3 as shown. However, the dark regions where no flame was present were clipped before tomographic inversion to save computational cost, resulting in an actual measurement volume of 16 × 16 × 16 cm^3 for the data shown here. The azimuth angles were θ = 0°, 21.66°, 90°, 119.25°, and $161.37^{0,}$ respectively for camera 1 through 5. Finally note that the results shown here were taken with Φ = 90° for all five cameras (i.e., in a coplanar fashion), with the intent of facilitating the intuitive interpretation of the results. Though as discussed in [11], such a coplanar configuration may not be optimal for the tomographic inversion. Figure 5 shows a set of 10 consecutive frames of the projections measured by camera 3for a duration of 10 ms. These projections were taken at a frame rate of 1 kHz, an exposure time of 1 ms, and a pixel resolution of 1024×1024. The

#202046 - $15.00 USD Received 5 Dec 2013; revised 27 Jan 2014; accepted 27 Jan 2014; published 21 Feb 2014
(C) 2014 OSA

temporal correlation between adjacent frames suggests that the temporal resolution in these measurements was sufficient to capture the dynamics of this flame.

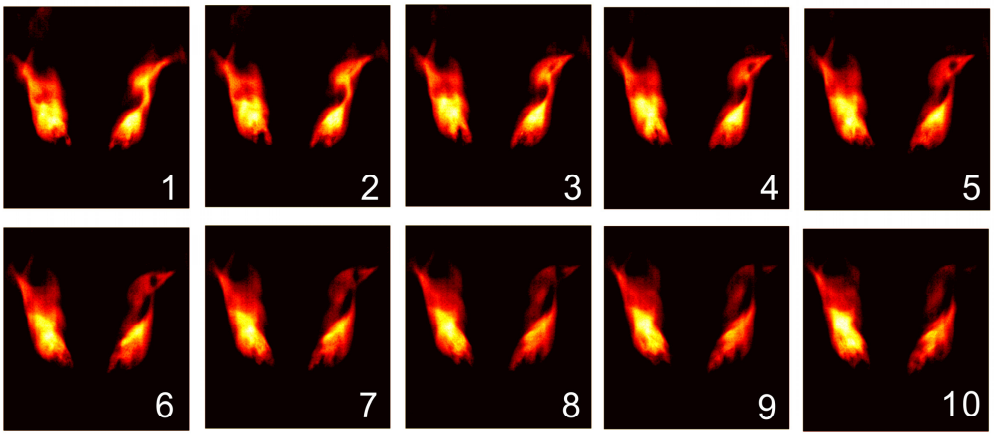

Fig. 5. 10 consecutive frames of projection measured by camera 3.

Using the projections shown in Fig. 4 as inputs, tomographic inversion was performed to obtain the 3D flame structures. Based on such 3D data, Fig. 6 shows a set of example rendering of the flame viewed from different orientations. These reconstructions were performed by discretizing the measurement volume into 64 × 64 × 64 (= 262,144) voxels, resulting in a spatial resolution of 2.5 mm in each direction. A 2 × 2 binning was first applied to the projections shown in Fig. 4 (whose original resolution is 1,024 × 1,024 pixels). After the clipping aforementioned and the binning, each camera provides ~2×10^5 equations in the form of Eq. (1). Thus, the projections from all five cameras provide a total of ~1 million equations to solve for the 262,144 unknowns, and the TISA algorithm [11] was applied to solve these questions. The discretization and the measurement setup were determined by consideration of the spatial resolution that is physically achievable and the computational cost. Both experimental results (as those shown in Fig. 3) and numerical simulation suggested an achievable spatial resolution of ~2 mm with five cameras. Tomography at this scale is computation and memory intensive. Obtaining one frame of 3D reconstruction as those shown in Fig. 6 requires solving a system of ~1 million equations, and the PSF at each view angle requires ~10 GB of memory storage. Research is ongoing to develop new tomographic algorithms that are efficient and scalable.

#202046 - $15.00 USD Received 5 Dec 2013; revised 27 Jan 2014; accepted 27 Jan 2014; published 21 Feb 2014
(C) 2014 OSA

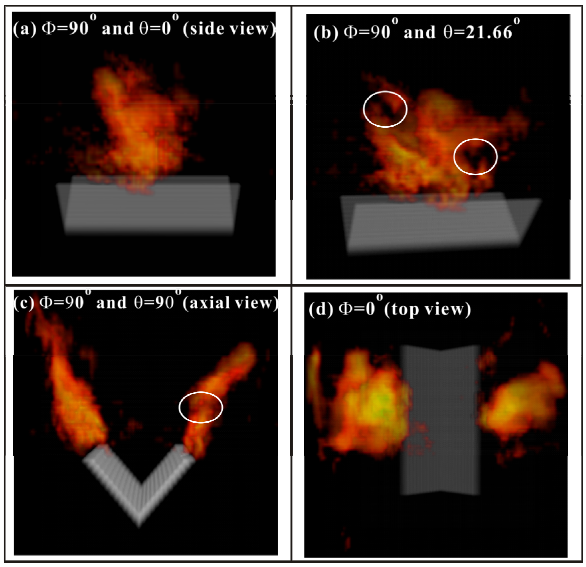

Fig. 6. Example 3D reconstructions (Media 1).

Accompanying the results in Fig. 6 is a media files (Media 1) that shows an animated 360° rotation view from Φ = 90° based on the 3D data used in Fig. 6. The results (the rendering and media) shown here illustrate TC's ability to obtain 4D flame measurements, also the challenge of visualizing high dimensional large data sets encountered in flow and flame measurements, a discussion beyond the scope of this current paper [28, 30]. Lastly, based on the 3D tomographic reconstruction, the flame can be viewed and studied from arbitrary orientations. For example, Fig. 7 shows the cross-sectional view of the flame on the *x-z* plane taken from 10 consecutive frames of the 3D reconstructions, each again obtained at 1 kHz frame rate and 1 ms exposure. The pixel resolution here was 64×64. The *y* position of these cross-sectional views was y = 0, i.e., along the center of the jet exit. The orientation of these cross-sectional views was therefore along the axis of the V-gutter, just as that of camera 3. These cross-sectional views again show the frame to frame temporal correlation, and comparing them with the projection data shown in Fig. 5 reveals features at this particular location that camera 3 was unable to resolved via line-of-sight measurements.

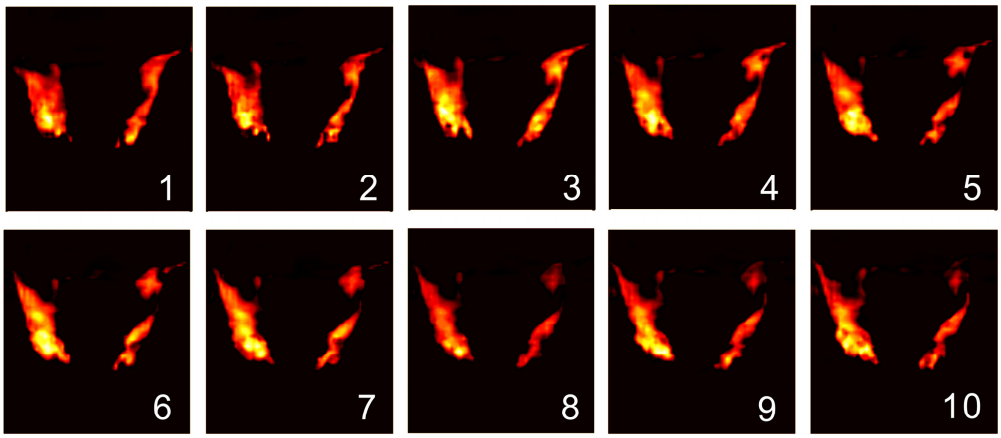

Fig. 7. Cross-sectional view from 10 consecutive 3D reconstructions.

#202046 - $15.00 USD Received 5 Dec 2013; revised 27 Jan 2014; accepted 27 Jan 2014; published 21 Feb 2014
(C) 2014 OSA

4. Validation of 3D measurements

It is difficult to directly and experimentally verify the 3D measurements as described above, and the results reported here were verified indirectly in several ways.

First, the experiments performed with a stable flame and the results shown in Fig. 3 verified TC's ability and achievable spatial resolution, and some intuitive verification can be obtained for the turbulent flame measurements by comparing the projections (shown in Fig. 4) and the reconstructions (shown in Fig. 6). As aforementioned, the results in Fig. 4 were intentionally taken with $\Phi = 90°$ to facilitate such comparison. The most intuitive comparison can be made between the projections on cameras 1 and 3 (Fig. 4) versus the side and axial view of the 3D reconstructions (Fig. 6(a) and 6(c), respectively). The projection from camera 1 suggests the flame is slightly tilted towards the left (at that moment), and that from camera 3 suggests the left branch of the flame is taller and larger than the right branch. These features are observed in the 3D reconstruction shown in Fig. 6(c) and 6(d). The top view (Fig. 6(d)) further confirms the left branch is larger than the right. Closer examination provides verification at a more detailed level. For instance, the projection measured by camera 2 shows some cavities in the flame when viewed from $\theta = 21.66°$, and these cavities were correctly captured by the reconstruction as highlighted by the circled regions in Fig. 6(b). As another example, the projection measured by camera 3 shows the right branch of the flame, when viewed axially, had two disjointed regions of intense combustion. The circled region in Fig. 6(c) correctly captured this feature.

Second, we have developed a ray tracing program to simulate the projection measurements based on the 3D tomographic reconstructions, and the simulated projections were in good agreements with those experimentally measured (which is necessary but not sufficient to verify the correctness of the tomography inversion). Figure 8 shows a comparison of the measured projections (as shown in Fig. 4) and the projections calculated via ray tracing based on the 3D reconstruction (as shown in Fig. 6). As seen, the comparison shows that the calculated projections agree with the measured projections both qualitatively and quantitatively, supporting the validity of the 3D measurements (again, not necessarily proving it).

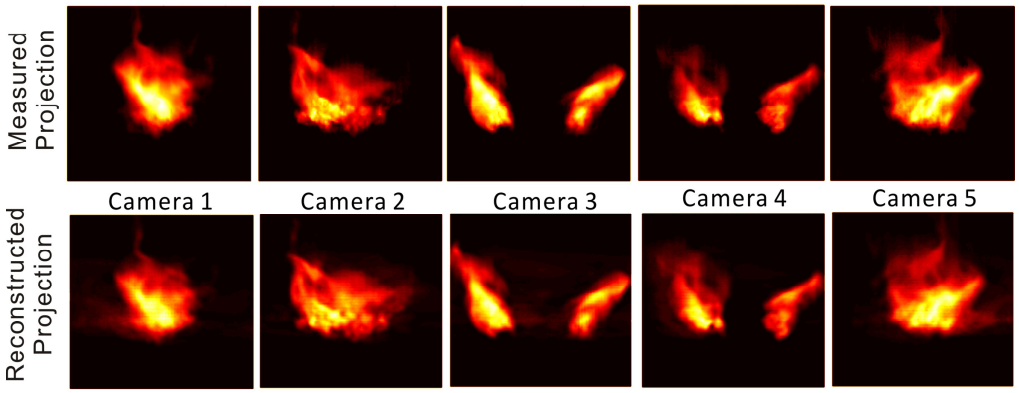

Fig. 8. Comparison of measured projections and projections calculated via ray tracing based on the 3D reconstruction.

Lastly, Fig. 9 shows computational results obtained with phantoms created to simulate the flames used in experiments. Phantoms have been created to simulate both the stable patterned flame as shown in Fig. 2(a), and also the turbulent V-flame as shown in Fig. 6. The results obtained showed similar trend, and therefore only those obtained with the turbulent V-flame are shown here in Fig. 9. In these simulations, projections were calculated according to Eq. (1) using the phantom as F. The calculated projections were then used as inputs in the tomographic algorithm to obtain 3D reconstructions. The uncertainties in the experimental measurements were estimated to be less than 5%. Therefore, these simulations were

#202046 - $15.00 USD Received 5 Dec 2013; revised 27 Jan 2014; accepted 27 Jan 2014; published 21 Feb 2014
(C) 2014 OSA

performed both with noiseless projections and also with 5% random Gaussian noise artificially added to the projections.

The advantage of using phantoms is that the fidelity of the reconstruction can be quantified by any criterion because the phantoms are known, and here we used the criterion of overall error (e) and correlation coefficients (r) as defined below:

$$e = \frac{\sum_{i_x}\sum_{i_y}\sum_{i_z}\left|F^{rec}_{i_x,i_y,i_z} - F_{i_x,i_y,i_z}\right|}{\sum_{i_x}\sum_{i_y}\sum_{i_z}\left|F_{i_x,i_y,i_z}\right|} \text{ and } r = \frac{\mathrm{cov}(FF^{rec})}{\sigma_F \sigma_{F^{rec}}} \tag{3}$$

where F represents the known phantom, F^{rec} the reconstruction, and σ_F and $\sigma_{F^{rec}}$ the std of F and F^{rec}, respectively. Additionally, these phantoms can also be generated to simulate small scale turbulent fluctuations (e.g., by using results from DNS, direct numerical simulations, as phantom) that are difficulty to generated in a controlled fashion experimentally. However, these phantom studies encounter the same computation and memory challenges as the analysis of the experimental data, really a generic challenge to all multi-scale and multi-dimensional problems in general. With the computational resources we have, these phantom studies were conducted under similar configurations as the analysis of the experimental data. The sought F was discretized into 64 × 64 × 64 (= 262,144) voxels, and projections were calculated with 500 × 500 (= 250,000) pixels. With 10 projections, the PSF has ~6×10^{11} (262,144 × 250,000 × 10) elements, a significant requirement on computational and memory resources.

These criteria defined in Eq. (3) reflect different aspects of the performance of the reconstruction: a perfect reconstruction results in e = 0%, and a perfect reconstruction that is different from the phantom by a shift results in r = 100%. Figure 9(a) and 9(b) show the e and r obtained in these simulations, respectively. These results shows that reconstruction performance increases (both reflected in decreasing e and increasing r) as more projections are available, corrugating the results shown in Fig. 3. Figure 9 also shows that with noiseless projections at 5 views, reconstruction with e = 2.5 and 5.8% can be obtained with noiseless projections and projections with 5% noise, respectively. Since the uncertainties in the measurements were estimated to be within 5%, the overall e for the experimental results shown in Fig. 6 was estimated to be between 2.5 and 5.8%. The overall error can be reduced either by reducing the measurement uncertainty or more cameras to obtain more projections. These results also provide insights into the effects of temporal resolution of the technique, as the measurement uncertainty improves with longer integration time (thusly slower temporal response). Furthermore, it becomes easier to gather more projections at more views at slower temporal resolution. Also note that Fig. 9(a) shows r is above 99% when five or more projections are used, indicating that a substantial portion of e may be due to a shift between the reconstruction and phantom, and a detailed analysis into the interpretation of these criteria are undergoing.

#202046 - $15.00 USD Received 5 Dec 2013; revised 27 Jan 2014; accepted 27 Jan 2014; published 21 Feb 2014
(C) 2014 OSA

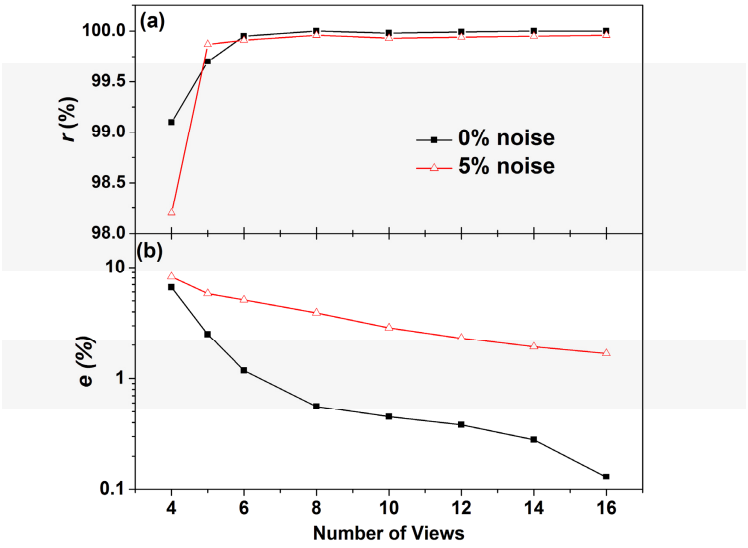

Fig. 9. Computational results obtained using phantom created to simulate the V-flame.

5. Summary

To summarize, this work studied the instantaneous flame measurements in 3D based on tomographic chemiluminescence (TC). Both experimental and computational studies have been conducted, with a focus on the quantification of the spatial resolution and fidelity of the 3D measurements. Experiments have been conducted both using stable flames with well-controlled patterns to study the spatial resolution, and also using turbulent flames to demonstrate instantaneous measurements at kHz rate in a relatively large volume of 16 × 16 × 16 cm^3 using five high speed cameras. Computations have been conducted using phantoms simulating the experimental flames for comparison and validation purposes. The simulation results suggest an overall reconstruction error within 5.8%, and a high degree of correlation. These simulation results, besides providing validation and uncertainty analysis to the experimental data, also provide insights into the effects of temporal resolution of the technique. Ongoing research efforts are investigating the relationship of the reconstruction error and the correlation, and designing new experiments and simulations that can be directly compared against the volumetric measurement. A possible strategy is to compare a cross-section of the 3D measurements against a 2D planar technique (such as PLIF, planar laser induced fluorescence).

Acknowledgement

The authors thank Dr. Yong Cao and Mr. Junpeng Wang (Computer Science, Virginia Tech) for their help with the rendering of the 3D data shown in Fig. 6. This article was supported by Virginia Tech's Open Access Subvention Fund.

#202046 - $15.00 USD Received 5 Dec 2013; revised 27 Jan 2014; accepted 27 Jan 2014; published 21 Feb 2014
(C) 2014 OSA